IMPLEMENTATION OF A PASSIVE RC LOW-PASS FILTER FOR EMBEDDED IOT SYSTEMS WITH OPEN-SOURCE SIMULATION SUPPORT

Submitted: 22.08.2025.

Accepted: 16.09.2025.

Hristina Delibašić-Marković¹, Violeta Petrović¹, Ivan Petrović²

¹University of Kragujevac, Faculty of Science, Radoja Domanovića 12, 34000 Kragujevac, Serbia, hristina.delibasic@pmf.kg.ac.rs

Coresponding author: Hristina Delibašić-Marković, University of Kragujevac, Faculty of Science, Radoja Domanovića 12, 34000 Kragujevac, Serbia, hristina.delibasic@pmf.kg.ac.rs

ABSTRACT

In this study, we explore the design, simulation, and deployment of a passive RC low-pass filter, specifically targeting its integration within Internet of Things (IoT) applications. We employed a symbolic computing environment to theoretically model the filter's frequency response, analytically deriving the transfer function and numerically validating it through simulation. Experimental verification was conducted using a virtual prototyping platform, where the filter was tested with various input signals. As a practical demonstration, the filter was implemented within a Python-based simulation of an IoT node, emulating a microcontroller setup for capturing analog signals with additive noise. The real-time processing of filtered outputs validated the filter's capacity to diminish high-frequency noise prior to digital conversion. This study highlights the ongoing importance of analog filtering techniques in enhancing data accuracy in contemporary IoT systems.

Keywords: RC low-pass filter, Internet of Things, numerical optimization.

INTRODUCTION

The IoT has transformed the way data is acquired, transmitted, and processed across numerous domains, from smart homes to industrial automation and environmental monitoring. At the core of these systems are sensor nodes that often operate under strict energy, size, and cost constraints. Despite the growing role of digital signal processing in embedded applications, analog signal conditioning remains a vital first step, particularly when high-frequency noise threatens to degrade the accuracy of analog-to-digital conversion. In such contexts, low-pass filters are usually employed to attenuate undesirable high-frequency components before digitization. By doing so, they help preserve the integrity of the measured signal and prevent aliasing. This is especially important in low-power devices where computational resources are limited, and software-based filtering is either infeasible or insufficient. Analog filtering, therefore, complements digital processing and plays an important role in maintaining data quality in IoT environments.

Recent studies have addressed the challenges of designing analog filters suitable for embedded systems. For example, authors in (Yuan et al., 2024) proposed an active RC low-pass and band-pass filter with automatic frequency tuning, enabling dynamic reconfiguration between Wi-Fi (Wireless Fidelity) and BLE (Bluetooth Low Energy) modes. Their work highlights the importance of tunability and integration in modern baseband circuits. In parallel, (Liao et al., 2022) developed a virtual low-pass filter for wind energy systems, where the filter was integrated into a power control loop to smooth output fluctuations without requiring physical filtering components. Both approaches illustrate how low-pass filtering, whether physical or emulated, can enhance system stability and performance across very different domains. Beyond active-RC designs, other analog filter topologies have also been investigated. For example, Gm-C filters, which rely on transconductance elements rather than discrete resistors, offer advantages in terms of compactness and bandwidth. However, they typically suffer from limited linearity and sensitivity to process variations, especially at low supply voltages (Ding et al., 2012). As a result, active-RC filters are

²Academy of Professional Studies Šumadija, Department in Kragujevac, Kosovska 8, 34000 Kragujevac, Serbia

often preferred in precision applications due to their improved noise and linearity characteristics. While such architectures are essential in high-performance systems, they may be unnecessary in simpler sensing tasks. In many IoT applications, where fixed bandwidth and low energy consumption are sufficient, passive RC low-pass filters offer a practical and efficient solution. Their minimal component count, predictable behavior, and ease of integration make them particularly attractive for early-stage signal conditioning. Motivated by this, the present study focuses on the design and simulation of a passive RC low-pass filter for use in IoT sensor nodes. The analysis combines symbolic modeling of the filter's frequency response with numerical simulations in Python. To complement the theoretical findings, a virtual prototyping environment is used to visualize the filter's behavior in time and frequency domains. Finally, the filter's performance is evaluated in a simulated IoT scenario, where it is applied to a noisy analog signal prior to digital conversion. Through this workflow, we aim to demonstrate that passive analog filtering remains highly relevant in contemporary embedded systems, not only due to its simplicity but also because of its measurable contribution to signal fidelity.

The remainder of this paper is organized as follows. Section 2 presents the theoretical foundation of the RC low-pass filter, including derivation of its transfer function and analysis of its frequency-domain behavior. Section 3 describes the numerical implementation and simulation results obtained using Python, with particular attention to signal smoothing in a simulated noisy environment. In Section 4, we introduce a virtual experimental setup developed in NI Multisim to visualize and validate the filter's behavior under different input conditions. Section 5 explores the integration of the filter into a Python-based IoT simulation framework, emulating real-world sensor data and analog preprocessing. Finally, Section 6 discusses the results, highlights the benefits and limitations of passive filtering in embedded applications, and outlines potential directions for future research.

THEORETICAL FRAMEWORK

A passive RC low-pass filter is a canonical example of a first-order linear time-invariant system, widely used for analogue signal conditioning. It consists of a resistor, R, in series with a capacitor C, where the output voltage, v_{out} , is taken across the capacitor. This configuration, presented in Fig. 1, suppresses high-frequency components of the input signal, v_{in} , while allowing low-frequency components to pass through with minimal attenuation (Li et al., 2017).

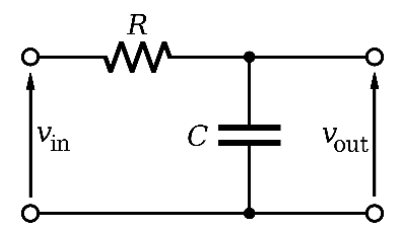


Figure 1. Schematic representation of a first order RC low-pass filter. The input voltage v_{in} is applied across the series combination of resistor R and capacitor C, with the output voltage v_{out} measured across the capacitor.

The behavior of the circuit presented in Fig. 1 is governed by Kirchhoff's voltage law (Coppens, et al., 2017):

$$v_{in}(t) = v_R(t) + v_C(t) \tag{1}$$

where the voltage drop across the resistor is given by Ohm's law as $v_R(t) = Ri(t)$, and the voltage across the capacitor relates to current by the integral relation $v_c(t) = \frac{1}{c} \int i(t) dt$. Using these expressions, we obtain the governing differential equation: $v_{in}(t) = RC \frac{dv_{out}(t)}{dt} + v_{out}(t) \qquad (2)$

$$v_{in}(t) = RC \frac{dv_{out}(t)}{dt} + v_{out}(t)$$
 (2)

To analyze the system in the frequency domain, we apply the Laplace transform to Eq. (2). This transformation requires assumptions about the system's initial state. For a passive filter that has not yet been energized, it is physically justified to assume that the capacitor is uncharged at t=0. This implies: $v_{out}(t=0)=0$. With this initial condition, the Laplace transform of the derivative becomes: $\mathcal{L}[dv_{out}(t)/dt] = sv_{out}(s)$. Applying the transform to Eq. (2) yields the algebraic relation:

$$v_{in}(s) = (sRC + 1)v_{out}(s)$$
 (3)

from which we obtain the transfer function:

$$H(s) = \frac{v_{out}(s)}{v_{in}(s)} = \frac{1}{1 + sRC}$$
 (4)

This parameter characterizes the system's response to sinusoidal excitation across all frequencies. For a steady-state sinusoidal input, we substitute $s = i\omega$ to obtain the frequency response:

$$H(j\omega) = \frac{1}{1 + j\omega RC}$$
 (5)

The magnitude and phase of this complex function are given by:

$$|H(j\omega)| = \frac{1}{\sqrt{1+(\omega RC)^2}}, \quad \angle H(j\omega) = -\tan^{-1}[\omega RC] \quad (6)$$

These expressions describe how the filter attenuates signals of different frequencies. At low frequencies $\omega \ll 1/RC$, the gain tends toward unity and the phase shift approaches zero. Conversely, at high frequencies $\omega \gg 1/RC$, the gain decreases proportionally to $1/\omega$, and the phase shift approaches $-\pi/2$.

The transition point between the passband and attenuation region is known as the cutoff angular frequency:

$$\omega_C = \frac{1}{RC} \qquad (7)$$

which corresponds to a frequency:
$$f_C = \frac{1}{2\pi RC}$$
 (8)

At this frequency, the magnitude drops to $-1/\sqrt{2} \approx 0.707$, corresponding to a power reduction of 50% or -3 dB. For applications involving signal analysis and logarithmic visualization, it is convenient to express the gain in decibels:

$$|H(j\omega)|_{dB} = -10 \log_{10}(1 + (\omega RC)^2)$$
 (9)

The slope of the Bode magnitude plot (see Section 3) asymptotically approaches -20 dB/ decade beyond the cutoff frequency, which is consistent with the first-order nature of the filter. The phase response similarly transitions from 0 to -90° , with the inflection point occurring at $\omega = \omega_{\mathcal{C}}$. This mathematical formulation provides a complete frequency-domain description of the RC low-pass filter. It serves as the analytical foundation for the numerical simulations and virtual prototyping to be discussed in the following sections.

NUMERICAL SIMULATION IN PYTHON

To assess the theoretical model under controlled conditions and to explore the RC filter's performance in typical IoT-like scenarios, we carried out a numerical simulation using Python. This enables us to track how the filter suppresses high-frequency noise and preserves the structure of low-frequency signals. Moreover, this method provides insight into signal behaviour prior to any physical implementation, which is particularly useful when designing embedded systems where testing is often constrained. Such numerical evaluations are frequently applied during early-stage development of sensor interfaces, especially in low-power systems where analogue preprocessing is tightly coupled with digital acquisition and conversion stages.

The simulation relies on a discrete-time formulation of the Eq. (2), derived in Section 2. Using a backward Euler approximation (Yeh et al., 2007), the system is represented by the recursive expression:

$$v_{out}[n] = v_{out}[n-1] + \alpha(v_{in}[n] - v_{out}[n-1]).$$
 (10)

with $\alpha = \Delta t/(RC + \Delta t)$, where Δt is the simulation time step. This relation imitates the dynamic behavior of the analog circuit and is numerically stable, making it suitable for digital implementation on microcontrollers. A synthetic input signal was constructed as the sum of a 5 Hz sine wave and additive white Gaussian noise, representing a simplified model of analogue sensor output contaminated by environmental interference. The filter was applied to this signal using the recursive relation (see Eq. (10)). As shown in Fig. 2, the output signal maintains the underlying structure of the sinusoid while significantly reducing high-frequency fluctuations.

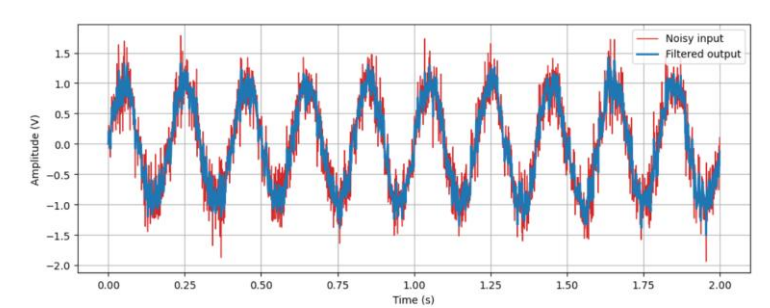


Figure 2. Simulated input (red) and filtered output (blue) in the time domain.

To quantify the effect of filtering, the signal-to-noise ratio (SNR) was calculated before and after applying the filter. The SNR was defined as (Mittal et al., 2024):

$$SNR = 10\log_{10} \left(\frac{\sigma_{signal}^2}{\sigma_{noise}^2} \right)$$
 (11)

where σ_{signal}^2 and σ_{noise}^2 denote the variances of the clean signal and noise, respectively. In our simulation, as shown in Fig.3, the initial SNR was approximately 7.68 dB, while the filtered output reached 12.34 dB, indicating a notable improvement in signal clarity.

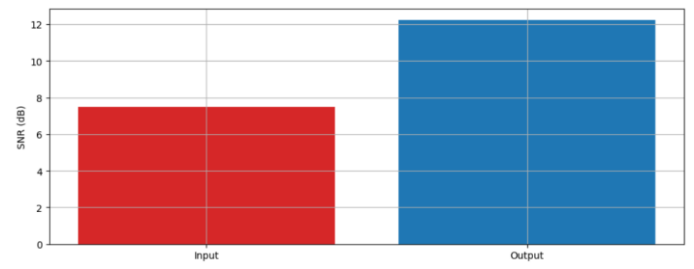


Figure 3. Signal-to-noise ratio before and after filtering.

To verify the frequency-domain behaviour of the RC low-pass filter, the magnitude response was first computed using the analytical expression given by Eq. (9). This function describes the gain in decibels as a function of angular frequency and reveals the characteristic profile of a first-order low-pass filter (Aye and Hla, 2025): constant gain at low frequencies and attenuation beyond the cutoff point.

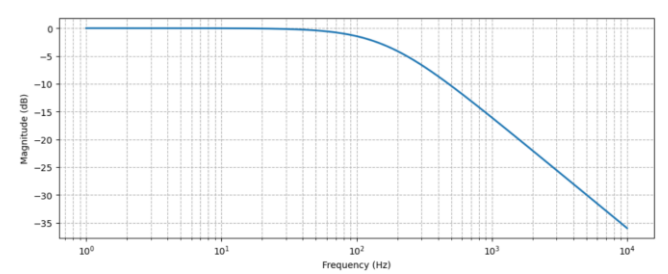


Figure 4. Theoretical Bode magnitude plot of the RC low-pass filter.

Fig. 4 shows the corresponding magnitude response obtained through numerical simulation of the discrete-time implementation. The curve exhibits a flat passband region followed by a smooth roll-off at higher frequencies, in line with the expected -20 dB per decade slope. This confirms that the discrete-time filter preserves the essential frequency-selective properties of its continuous counterpart, making it suitable for noise suppression in embedded signal acquisition systems.

VIRTUAL PROTOTYPING IN NI MULTISIM

To complement the analytical and numerical analyses, a virtual prototype of the RC low-pass filter was constructed in NI Multisim. This environment allows for realistic circuit simulation based on SPICE models and provides tools for both time-domain and frequency-domain evaluation. The objective was to replicate the filter behaviour under conditions that closely resemble hardware implementation, using the same component values adopted in previous sections ($R=1~k\Omega$, $C=1~\mu F$). Unlike the Python simulation in Section 3, which incorporated synthetic noise to model sensor-level disturbances, the Multisim simulations focus exclusively on the behaviour of the circuit. By removing noise, we isolate the effect of the filter components and better visualize how signal characteristics change solely due to variations in capacitance. The schematic used in the simulation is shown in Fig. 5. A 5 Hz sine wave of 1 V is applied to the RC network using a function generator (XFG1). The output is observed across the capacitor using a virtual oscilloscope (XSC1).

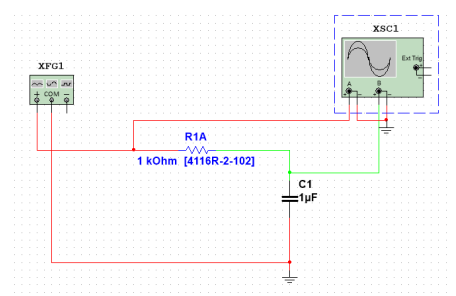


Figure 5. Schematic of the RC low-pass filter simulated in NI Multisim ($R = 1 \text{ k}\Omega$, $C = 1 \text{ \mu}F$).

The measured input and output waveforms for two capacitance values are shown in Fig. 6. With $C=1~\mu F$, the output signal (green trace) closely follows the input (red trace), with minor attenuation and a small phase lag. This behavior is consistent with the fact that the input frequency (5 Hz) is much lower than the cutoff frequency of the filter, $f_C=1/2\pi RC\approx 159~\text{Hz}$, so most of the signal passes through unaltered. When the capacitance is increased to $10~\mu F$, the cutoff frequency drops to approximately 15.9 Hz. Although the input frequency remains the same, it is now closer to the filter's corner frequency. As a result, the circuit responds more gradually: the output becomes smoother, attenuated, and increasingly delayed in phase. Physically, this reflects the greater energy storage capacity of the larger capacitor, which charges and discharges more slowly, effectively dampening rapid voltage changes.

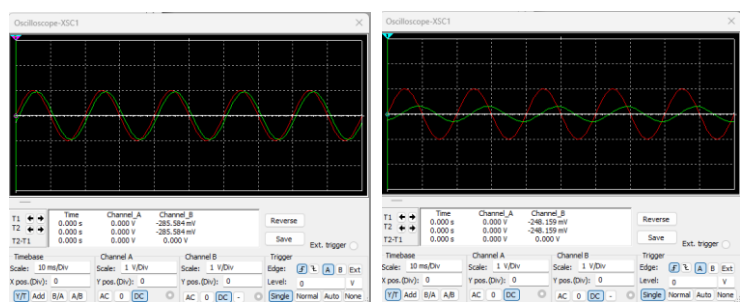


Figure 6. Comparison of time-domain responses for $C=1~\mu F$ (left) and $C=10~\mu F$ (right). Increasing capacitance introduces stronger attenuation and phase lag, reflecting the slower charging dynamics of the capacitor.

The results presented in Fig. 6 highlight a fundamental trade-off in RC filtering: increasing capacitance enhances noise suppression and signal smoothing but also introduces a delay and attenuates even low-frequency components if the cutoff becomes too low.

To analyse the frequency response, we used Multisim's Bode plot tool. Fig. 7 shows the magnitude plots for both configurations. The classic first-order roll-off of $-20 \, \mathrm{dB/decade}$ is evident in both cases, with a clear shift of the cutoff frequency when C increases. This confirms that the filter's bandwidth is inversely proportional to the RC product and that tuning C enables flexible control over the signal passband.

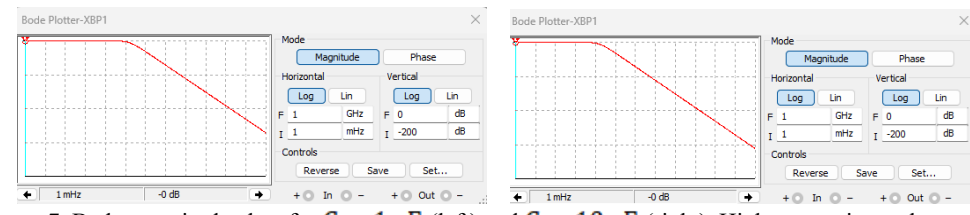


Figure 7. Bode magnitude plots for $C = 1 \,\mu\text{F}$ (left) and $C = 10 \,\mu\text{F}$ (right). Higher capacitance lowers the cutoff frequency, narrowing the filter's bandwidth.

Together, the simulations presented in this section demonstrate how passive RC filters shape the temporal and spectral characteristics of signals. Even in idealized conditions, the observed behaviours align well with theoretical predictions and provide a useful foundation for implementing such filters in real-world analog or embedded systems.

INTEGRATION INTO PYTHON-BASED IOT SIMULATION FRAMEWORK

Following the theoretical, numerical, and virtual analyses presented in previous sections, we now turn to a practical scenario in which the RC low-pass filter is integrated into a simulated IoT sensor node. While Section 3 explored the filter's numerical behaviour using synthetic signals and Section 4 offered a component-level perspective through virtual prototyping in NI Multisim, this section bridges the gap between simulation and application by emulating a simplified embedded sensing system.

In this section, we recreate a situation common in real-world IoT deployments: a sensor provides continuous analog readings of a slowly varying physical quantity, such as temperature or pressure, which are then contaminated by environmental or electronic noise. Before this signal can be digitized and processed, analog filtering is typically employed to reduce high-frequency interference that could compromise measurement accuracy or exceed the ADC's bandwidth. To realistically model this process, the clean sinusoidal signal obtained in Section 4 via Multisim was adopted as the true reference signal, the ideal physical variable we aim to measure. Gaussian noise was numerically added to simulate the distortions encountered in real-world sensing. The resulting signal thus mimics a corrupted analog input to a microcontroller. This noisy waveform was then passed through the recursive digital filter implemented in Section 3, using the same values for resistance and capacitance ($R = 1 \text{ k}\Omega$, $C = 1 \mu\text{F}$), ensuring direct comparability with earlier results. The outcome of this simulation is shown in Fig. 8. The red curve represents the noisy signal, whose high-frequency fluctuations obscure the true dynamics of the underlying physical quantity. The black dashed line corresponds to the original, noise-free signal reused from the virtual experiment in Multisim. The blue curve shows the output of the filtering process. It is evident that the filtered signal follows the slow variations of the original waveform, while the fast oscillations are effectively suppressed. This confirms the filter's ability to enhance signal quality by isolating relevant low-frequency components and rejecting high-frequency noise.

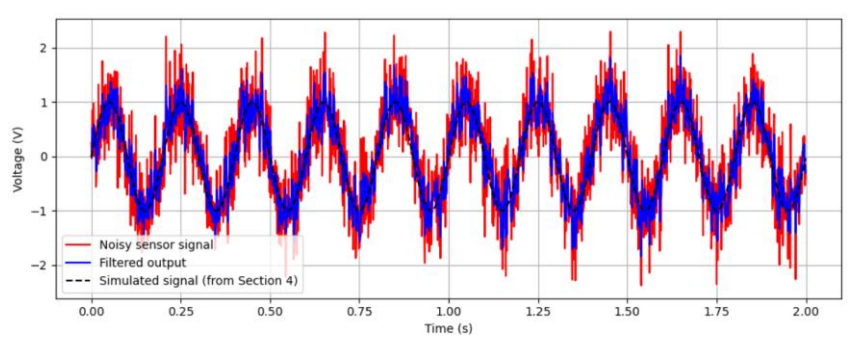


Figure 8. Simulated sensor acquisition in a Python-based IoT node. The red curve represents a noisy input signal. The blue curve is the filtered output using the RC low-pass filter. The black dashed line denotes the original signal waveform extracted from the Multisim simulation in Section 4.

The result presented in Fig. 8 confirms the low-pass behavior of the RC filter. The signal components at low frequencies (around 5 Hz in this case) are transmitted almost undistorted, while rapid fluctuations introduced by noise (which span a broad frequency range) are heavily attenuated. This selectivity stems from the fact that the capacitor's reactance decreases with frequency, shunting high-frequency components away from the output node. As a result, the filter's output predominantly consists of the frequency components within the passband, with minimal contribution from higher frequencies. This experiment reinforces the practical utility of analog

filtering in IoT systems. Even in the presence of significant noise, a simple first-order RC circuit provides meaningful improvement in signal clarity without requiring additional digital resources or power. The filtering operation is local, passive, and computationally free making it ideal for constrained edge devices. Furthermore, by using the same reference waveform as in Multisim simulations, we verify that the filter's performance translates consistently across different implementation layers, from physical hardware to software reproduction.

CONCLUSIONS

This paper explored the behavior and practical utility of a passive RC low-pass filter across theoretical, numerical, and simulated environments. Starting from the differential equation model, we derived the filter's transfer function and described its response in both time and frequency domains. Python-based simulations showed that the filter significantly improves signal clarity by attenuating high-frequency noise. These results were consistent with the expected -20 dB per decade roll-off and the preservation of low-frequency content. The filter was then implemented in a virtual NI Multisim environment, using identical component values. The comparison between different capacitances illustrates how increasing capacitance lowers the cutoff frequency, enhancing filtering while introducing more delays. These trends aligned well with analytical predictions and offered insight into real-world circuit behavior. Finally, we integrated the filter into a simplified IoT simulation. A noisy sensor signal was passed through the RC circuit before digitization. The output confirmed that analog filtering remains a valuable preprocessing step, particularly for low-power systems where digital resources are limited. By using the same reference waveform throughout all stages, we ensured consistency across theory, simulation, and practical modeling. In summary, even a simple passive filter can provide meaningful improvements in signal quality. Its predictable behavior, low cost, and zero computational load make it well suited for embedded and IoT applications. Future work could involve physical implementation on microcontrollers, exploration of adaptive filter tuning, or extension to higherorder analog networks.

ACKNOWLEDMENTS

Authors would like to acknowledge the support received from the Science Fund of the Republic of Serbia, #GRANT 6821, Atoms and (bio) molecules-dynamics and collisional processes on short time scale - ATMOLCOL. Our appreciation also goes to the Serbian Ministry of Education, Science and Technological Development (Agreement No. 451-03-136/2025-03/200122). H. Delibašić Marković would also like to express gratitude to COST Actions CA21159 - "Understanding interaction of light with biological surfaces: possibility for new electronic materials and devices" for their support and CA22148 - "An international network for Non-linear Extreme Ultraviolet to hard X-ray techniques (NEXT)".

DECLARATIONS OF INTEREST STATEMENT

The authors affirm that there are no conflicts of interest to declare in relation to the research presented in this paper

LITERATURE

- Aye, M. and Hla, T. T. (2025). Identification of characteristics for RC Low Pass, High Pass, Band Pass and Band Stop Filters. *The Indonesian Journal of Computer Science*, 14(2).
- Coppens, P., Van den Bossche, J. and De Cock, M. (2017). Student understanding of first order RC filters. *American Journal of Physics*, 85(12), 937–947.
- Ding, L. S., Yu, J. C. and Hong, W. C. (2012). A linearized technique in an all-MOS transconductance amplifier. *Microelectronics Journal*, 43(11), 1023–1028.
- Li, D., Basak, D., Zhang, Y., Fu, Z. and Pun, K. P. (2017). Improving power efficiency for active-RC delta-sigma modulators using a passive-RC low-pass filter in the feedback. *IEEE Transactions on Circuits and Systems II: Express Briefs*, 65(11), 1559–1563.

- Delibašić-Marković, H., et al. (2025). Implementation of a passive RC low-pass filter for embedded IOT systems with open-source simulation support. *STED Conference* 14(2), 505-513.
- Liao, K., Lu, D., Wang, M. and Yang, J. (2022). A low-pass virtual filter for output power smoothing of wind energy conversion systems. *IEEE Transactions on Industrial Electronics*, 69(12), 12874–12885.
- Mittal, N., Khan, I. U. and Khan, Z. H. (2024). Design a low-power low-pass nano dimension-based filter with high linearity for next-generation WSN. *International Journal of Nano Dimension*, 15(4 (October 2024)), 1–10.
- Yeh, D. T., Abel, J. and Smith, J. O. (2007). Simulation of the diode limiter in guitar distortion circuits by numerical solution of ordinary differential equations. *Proceedings of the Digital Audio Effects (DAFx'07)*, 197–204.
- Yuan, S., Xuan, H., Feng, H. and Tang, X. (2024). Scalable, low-power and high-performance active-RC complex band-pass/low-pass filter with automatic frequency tuning applied to the Internet of Things. *Microelectronics Journal*, 153, 106430.